

Available online at www.sciencedirect.com

International Journal of Solids and Structures 44 (2007) 4909–4924

INTERNATIONAL JOURNAL OF
**SOLIDS and
STRUCTURES**www.elsevier.com/locate/ijssolstr

Electromigration induced strain field simulations for nanoelectronics lead-free solder joints

Cemal Basaran *, Minghui Lin

Electronic Packaging Laboratory, Department of Civil, Structural and Environmental Engineering, University at Buffalo, State University of New York, 212 Ketter Hall, Buffalo 14260, USA

Received 7 June 2005; received in revised form 5 December 2006

Available online 15 December 2006

Abstract

Electromigration is a major road block on the way to realization of nanoelectronics. Determination of plastic deformation under high current density is critical for prediction of electromigration failure. A new displacement–diffusion coupled model is proposed and implemented using finite element method. The model takes into account viscoplastic behavior of solder alloys, as a result, vacancy concentration evolution and electromigration process are accurately simulated. Finite element simulations were performed for lead-free solder joints under high current density and compared with experimental moiré interferometry measurements. The comparison validates the model.

© 2006 Elsevier Ltd. All rights reserved.

Keywords: Electromigration; Thermomigration; Viscoplasticity; Current crowding; Finite element method; Nanoelectronics packaging

1. Introduction

Electromigration is a major reliability concern for nanoelectronic packaging. This is especially true for solder joints with a height below 10 micron, which are necessary for nanoelectronics packaging. Electromigration is a biased diffusion process and the failure mechanism of electromigration is rather complicated in solder alloys and is usually accompanied with micro structural evolution. However, the main failure phenomenon, void nucleation due to electromigration, has a direct relationship with stress and strain (especially plastic strain) state of the specimen (Goods and Brown, 1978; Gleixner and Nix, 1996). The state of stress during the electromigration determines the counter flow of mass due to influence of stress gradient and vacancy gradient (Blech, 1998). Thus computational simulation of strain and stress evolution during electromigration is essential for failure prediction. Some efforts have been made to model and simulate stress evolution due to electromigration, which include some analytical solutions and numerical implementations (Park et al., 1999; Ye et al., 2003; Korhonen et al., 1993; Sarychev and Zhinikov, 1999). A big disadvantage of the models available in the literature is that they treat materials as elastic for simplification, although materials such as

* Corresponding author. Tel.: +1 716 645 2114; fax: +1 716 645 3733.
E-mail address: cjb@buffalo.edu (C. Basaran).

aluminum, copper and solder alloys exhibit a great deal of plasticity. In this paper, a fully coupled displacement–diffusion model with nonlinear mechanical material properties (plasticity or viscoplasticity) is proposed and implemented with finite element method. The finite element simulations of electromigration induced strain fields in lead-free solders using this model are conducted. The simulation results are compared with experimental moiré interferometry measurements.

2. Electromigration model formulation

A number of theoretical models have been developed to describe electromigration induced stress evolution (Korhonen et al., 1993; Sarychev and Zhinikov, 1999). Here Sarychev and Zhinikov (1999) approach is adopted to model the vacancy diffusion under electromigration. The volumetric strain in the lattice caused by vacancy divergence is comparable to traditional thermal volumetric strain. According to Sarychev and Zhinikov (1999) theory in a lattice when an atom moves to a new site, due to electromigration forces, it leaves behind a vacancy. The difference between the volume of an atom and the volume of a vacancy leads to volumetric strain at that lattice site. The proposed solder alloy constitutive model has viscoplasticity with nonlinear isotropic/kinematic hardening capabilities. A user defined element subroutine is coded for ABAQUS (a general purpose finite element software) to solve coupled equations of displacement and diffusion fields. The details of finite element algorithm and formulation are presented in another paper (Lin and Basaran, 2005) and are omitted here. Integration algorithm for nonlinear kinematic/isotropic hardening is based on Lubarda and Benson (2002).

2.1. Governing equations

Electromigration is diffusion controlled mass transport process. It is governed by the following vacancy conservation equation which is equivalent to mass conservation equation

$$\int_v \left(C_{v0} \frac{\partial c}{\partial t} + \nabla \cdot \mathbf{q} - G \right) dV = 0, \quad (1)$$

where C_{v0} is equilibrium vacancy concentration in the absence of a stress field, c is normalized vacancy concentration and $c = \frac{C_v}{C_{v0}}$, C_v is vacancy concentration, t is time, \mathbf{q} is vacancy flux, a vector and G is vacancy generation/annihilation rate.

Force equilibrium is governed by Cauchy's equation of motion

$$\nabla \cdot \boldsymbol{\sigma} + \mathbf{k} \mathbf{b} = \mathbf{k} \frac{d\mathbf{v}}{dt}, \quad (2)$$

where $\boldsymbol{\sigma}$ is stress tensor, \mathbf{k} is material density, \mathbf{b} body force vector and \mathbf{v} displacement vector.

2.2. Constitutive equations

2.2.1. Diffusion model

Driving forces of vacancy flux are (i) vacancy concentration gradient, (ii) electrical field forces, (iii) stress gradient and (iv) thermal gradient. The vacancy flux is (Sarychev and Zhinikov, 1999; Basaran et al., 2003)

$$\mathbf{q} = -D_v C_{v0} \left(\nabla c + \frac{Z^* e}{kT} (-\rho \mathbf{j}) c + \frac{cf\Omega}{kT} \nabla \sigma_{\text{spherical}} + \frac{c}{kT^2} Q^* \nabla T \right), \quad (3)$$

where D_v is vacancy diffusivity, Z^* is vacancy effective charge number, e is electron charge, ρ is metal resistivity, \mathbf{j} is current density (vector), f is vacancy relaxation ratio, ratio of atomic volume to the volume of a vacancy, Ω is atomic volume, k is Boltzmann's constant, T is absolute temperature, $\sigma_{\text{spherical}}$ is spherical part of stress tensor, $\sigma_{\text{spherical}} = \text{trace}(\boldsymbol{\sigma}_{ij})/3$ and Q^* is heat of transport, the isothermal heat transmitted by moving the atom in the process of jumping a lattice site less the intrinsic enthalpy.

The stress–vacancy relationship is represented by vacancy generation/annihilation rate which is given by (Sarychev and Zhinikov, 1999)

$$G = -C_{v0} \frac{c - C_{ve}}{\tau_s} \tag{4}$$

where $C_{ve} = e^{\frac{(1-f)\Omega\sigma_{spherical}}{kT}}$ is normalized thermodynamic equilibrium vacancy concentration, τ_s is characteristic vacancy generation/annihilation time.

2.2.2. Displacement model

The stress–strain constitutive model is established on small strain assumption,

$$\sigma = C(\epsilon_{total} - \epsilon_{viscoplastic} - \epsilon_{electromigration} - \epsilon_{thermal}), \tag{5}$$

where $C = \kappa 1 \otimes 1 + 2\mu(I - \frac{1}{3}1 \otimes 1)$ and κ is bulk modulus, μ is shear modulus; and

$$I = \begin{bmatrix} 1 & 0 & 0 & 0 & 0 & 0 \\ 0 & 1 & 0 & 0 & 0 & 0 \\ 0 & 0 & 1 & 0 & 0 & 0 \\ 0 & 0 & 0 & 0 & 0 & 0 \\ 0 & 0 & 0 & 0 & 0 & 0 \\ 0 & 0 & 0 & 0 & 0 & 0 \end{bmatrix}, \quad 1 = \begin{bmatrix} 1 \\ 1 \\ 1 \\ 0 \\ 0 \\ 0 \end{bmatrix}.$$

Thermal strain is included as a field variable in current formulation. In the system under high current density, thermal equilibrium is reached much faster than diffusion process. Therefore, thermal analysis and diffusion analyses can be done separately, in a sequence, rather than concurrently. Thus the thermal strain can easily be added into the simulation from the results of an independent thermal-displacement analysis. The same approach is taken also for de-coupling electromagnetic field analysis from diffusion analysis. Current density is not uniform in the solder joint. Hence an electromagnetic field analysis is conducted first to determine the current density distribution in the solder joint, which results are then used as an input for a coupled displacement–diffusion analysis.

Itemized strain components are given as follows:

$$\epsilon_{total} = \frac{1}{3}\epsilon_{total}^{trace} \cdot 1 + \epsilon_{total}^{dev} \tag{6}$$

$$\epsilon_{viscoplastic} = \frac{1}{3}\epsilon_{viscoplastic}^{trace} \cdot 1 + \epsilon_{viscoplastic}^{dev} = \epsilon_{viscoplastic}^{dev} \tag{7}$$

$$\epsilon_{electromigration} = \frac{1}{3}\epsilon_{electromigration}^{trace} \cdot 1 + \epsilon_{electromigration}^{dev} = \frac{1}{3}\epsilon_{electromigration}^{trace} \cdot 1, \tag{8}$$

$$\epsilon_{thermal} = \frac{1}{3}\epsilon_{thermal}^{trace} \cdot 1 + \epsilon_{thermal}^{dev} = \frac{1}{3}\epsilon_{thermal}^{trace} \tag{9}$$

Substituting Eqs. (6)–(9) into Eq. (10) obtain

$$\sigma = \kappa \cdot (\epsilon_{total}^{trace} - \epsilon_{electromigration}^{trace} - \epsilon_{thermal}^{trace}) \cdot 1 + 2\mu(\epsilon_{total}^{dev} - \epsilon_{viscoplastic}^{dev}), \tag{10}$$

where $\epsilon_{electromigration}^{trace}$ is described by following equation (Sarychev and Zhinikov, 1999):

$$\frac{\partial \epsilon_{electromigration}^{trace}}{\partial t} = \Omega C_{v0}(f\nabla \mathbf{q} + f'G), \tag{11}$$

$$f' = 1 - f.$$

According to Sarychev and Zhinikov (1999) it is assumed that when an atom is replaced by a vacancy there is a local spherical strain introduced at that atomic lattice site due to difference between the volume of an atom and volume of a vacancy. Electromigration introduced strain happens due to following reasons:

- (1) vacancy flux divergence,
- (2) vacancy generation.

Using Eq. (1), we can transform Eq. (11) into

$$\frac{\partial \epsilon_{\text{electromigration}}^{\text{trace}}}{\partial t} = \Omega C_{v0} \left(G - f \frac{\partial c}{\partial t} \right) = \Omega C_{v0} \left(\frac{e^{\frac{(1-f)\Omega \sigma_{\text{spherical}}}{kT}} - c}{\tau_s} - f \frac{\partial c}{\partial t} \right). \quad (12)$$

Eqs. (10) and (12) plus J_2 plastic flow theory combined together yield the constitutive material behavior.

Neu et al. (2000) proposed a viscoplastic flow rule for Sn–Ag lead-free solder alloys based on McDowell's (1992) Unified Creep Plasticity (UCP) model

$$\dot{\epsilon}_{\text{viscoplastic}}^{\text{dev}} = A \left(\frac{\langle F \rangle}{D_r} \right)^n \exp \left[\left(\frac{F}{D_r} \right)^{n+1} \right] e^{-Q/R\theta} \frac{\partial F}{\partial \sigma}, \quad (13)$$

where the material parameters are defined as follows: A is a dimensionless material parameter to describe the strain rate sensitivity, $e^{\left(-\frac{Q}{R\theta}\right)}$ is an Arrhenius exponential for temperature dependency, Q is the creep activation energy for plastic flow; R is the universal gas constant = 8.314 J/K mol = 8.314 N mm/K mol; θ : absolute temperature in Kelvin; D_r : Creep drag strength, F is a over stress defined as $F = \|S - X\| - K(\alpha)$, S is a deviatoric stress tensor is given by $S = \sigma - \frac{1}{3}\text{Tr}(\sigma)1$, n is a stress exponent for viscoplastic deformation rate.

Neu et al.'s (2000) model uses a rather complicated back stress evolution function, after simplification, we propose using the following hardening evolution. Ignoring long range term, which is negligible compared with other terms, in the back stress evolution function. a kinematic hardening function similar to the one proposed by Armstrong and Frederick (1966) and Chaboche (1989) is obtained:

$$\dot{\alpha} = \sqrt{\frac{2}{3} \dot{\epsilon}_{\text{viscoplastic}}^{\text{dev}} \cdot \dot{\epsilon}_{\text{viscoplastic}}^{\text{dev}}}, \quad (14)$$

$$\dot{X} = c_1 \dot{\epsilon}_{\text{viscoplastic}}^{\text{dev}} - c_2 X \dot{\alpha}, \quad (15)$$

where c_1 is linear kinematic hardening constant, c_2 is nonlinear kinematic hardening constant, $\dot{\epsilon}_{\text{viscoplastic}}^{\text{dev}}$ is viscoplastic strain rate tensor, X is a back stress tensor defining the displacement of the center of the yield surface in the deviatoric stress space.

$K(\alpha)$ represents the isotropic hardening component defining the radius of the yield surface in stress space.

3. Finite element simulation

The test data used for validation was provided by Ye et al. (2003, 2004). Using the high sensitivity moiré interferometry technique, in situ displacement fields were recorded during the electrical current loading. In the following section, the moiré interferometry results and finite element simulation results are compared for displacement and strain fields.

3.1. Test vehicle assembly

Test sample details are shown in Figs. 1 and 2 where the optical table under the specimen is not shown. By means of optical diffraction grating attached on the surface of solder joints the images of the fringes are recorded in situ in real time throughout the whole current stressing process. The temperature fluctuation is controlled within 4° (Ye et al., in press).

3.2. 2 Finite element model

Finite element model is shown in Fig. 3. Copper plates and solder joints are modeled with 8 node plain strain element with thickness.

Copper plate thickness is 40 times the solder joint's thickness. Displacement boundary conditions at the left and right ends of copper plates are fixed in both horizontal, 1, (x) and vertical, 2, (y) directions. The diffusion boundary conditions between copper and solder joint are considered to be free. This means copper plate and

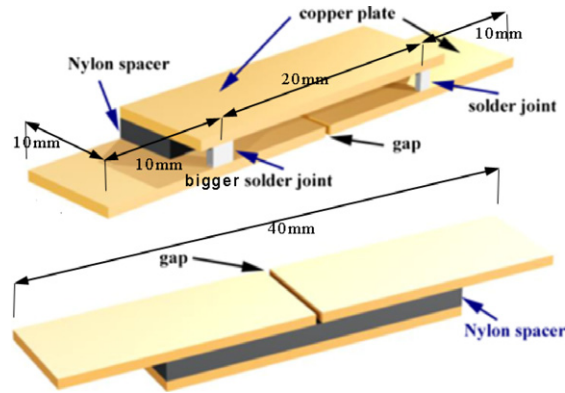


Fig. 1. Test sample detail.

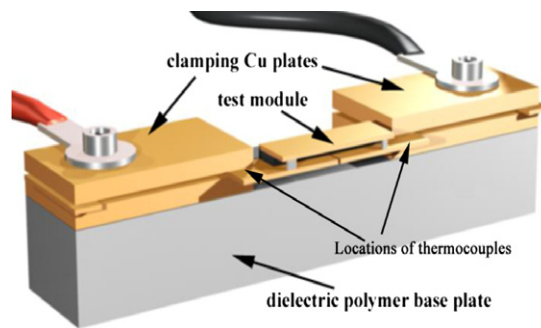


Fig. 2. Electrical connection for test sample.

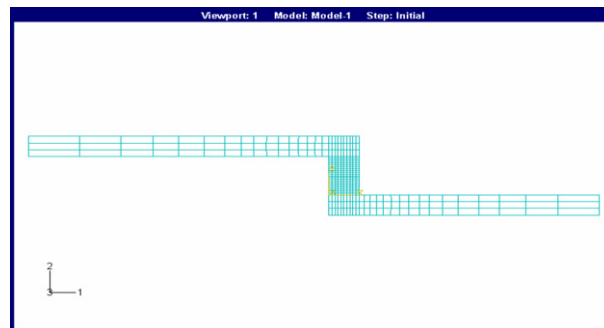


Fig. 3. Finite element mesh.

solder alloy can inter diffuse into each other. This assumption will be discussed in detail further in the later part of the paper.

3.3. Determination of material properties

95.5Sn/4Ag/0.5Cu lead-free solder is used in the tests. Sn is considered to be main diffusion specie (Ye, 2004).

3.3.1. Mechanical material properties

For lead-free solder, the mechanical material properties of the solder alloy are obtained from Neu et al. (2000). Elastic properties as well as kinematic hardening parameters and viscoplastic flow function parameters are shown in Table 1.

Table 1
Kinematic hardening and viscoplastic flow function parameters

| Parameter | Value |
|-----------------------|---|
| Young's Modulus | $E(T) = 45.0 - 9.0 \tanh[0.028 (T(K) - 298)]$ GPa |
| Poisson ratio | 0.4 |
| Uniaxial yield stress | 3.0 MPa |
| c_1 (MPa) | 9626.5 |
| c_2 | 725.1 |
| D_r | 3.0 MPa |
| n | 3 |
| A | 0.55 |
| Q (kJ/mol) | 50.0 |

3.3.2. Diffusion material properties

3.3.2.1. *Equilibrium vacancy concentration.* The atomic volume, Ω , of tin is $16.3 \text{ cm}^3/\text{mol}$ or $2.71 \times 10^{-23} \text{ cm}^3/\text{atom}$. The atomic concentration, C_a , of tin is $3.69 \times 10^{22}/\text{cm}^3$. The equilibrium vacancy concentration at a stress-free state is reported as by Balzer and Sigvaldason (1979), or $C_{v0} = 1.11 \times 10^{18}/\text{cm}^3$.

3.3.2.2. *Vacancy diffusivity.* Pure tin grain boundary diffusivity is reported by Prabjit and Milton (1984) by assuming a grain boundary width of 0.5 nm

$$D_{gb} = (4.9_{-3.7}^{+15.6}) \exp[-(11700 \pm 840 \text{ cal/mol})/RT] \text{ cm}^2/\text{s}$$

where $R = 8.3145 \text{ J/mol K} = 1.987 \text{ cal/mol}$, is gas constant, and T is absolute temperature. Diffusivity at grain boundary for tin is larger than lattice diffusivity by an order of magnitude, therefore in this simulation, the grain boundary diffusion is assumed to be the main diffusion mechanism in electromigration. By assuming an average grain size of $d = 300 \text{ nm}$ (Prabjit and Milton, 1984), the effective atomic diffusivity is thus found to be

$$D_a = \frac{\delta}{d} D_{gb} = \frac{0.5 \text{ nm}}{300 \text{ nm}} \times 4.9 \times \exp(-11700 \text{ cal}/RT) \text{ cm}^2/\text{s}.$$

At 300 K, D_a is calculated to be $2.97 \times 10^{-11} \text{ cm}^2/\text{s}$. The vacancy diffusivity is calculated from the relation Clement and Thompson, 1995, $D_a C_a = D_v C_v$, at the stress-free state. By assuming Balzer and Sigvaldason, 1979, $D_v = D_a / (3 \times 10^{-5}) = 1 \times 10^{-6} \text{ cm}^2/\text{s}$ is derived and used in the following simulations.

3.3.2.3. *Effective charge number Z^* .* The effective charge number of lead-free solder alloy is chosen as -10 at 30°C (measured stressing temperature), Prabjit and Milton, 1984. This negative effective charge number is for the atoms in the solder, indicating that the atoms are actually migrating in the opposite direction of electric current. Since the vacancy migrates in the opposite direction of the moving atom, the effective charge number for the vacancy is positive. Therefore, in the simulation the effective charge number of vacancy is taken as 10.

3.3.2.4. *Other simulation parameters for lead-free solder alloy.* All the material parameters regarding diffusion are summarized below in Table 2.

4. Numerical simulation results

4.1. Numerical simulation Case 1

For this case study, the electrical current density is $1.12 \times 10^4 \text{ A/cm}^2$. The current direction is from top to bottom. The solder joint has a non uniform thickness, as a result the current density is not constant along the height of the solder joint. This gradient of current density is taken into consideration in the numerical simulation and it turns out that, current density gradient is an essential part of loading. Non uniform thickness of solder joint is shown in Fig. 4.

The variation of the thickness of solder joint along its height can be formulated as

Table 2

Diffusion materials parameters

| | |
|--|--|
| Temperature | 303 K |
| τ_s = Vacancy relaxation time (TS) | $1.8E-3$ s (Sarychev and Zhinikov, 1999) |
| Diffusivity (D) | $100.0 \mu\text{m}^2 \text{s}^{-1}$ |
| Effective charge number (Z^*) | 10 |
| Electrical resistivity (ρ) | $1.15E-5 \Omega\text{cm}$ |
| Average vacancy relaxation ratio (f) | 0.6 (Sarychev and Zhinikov, 1999) |
| Atomic volume of tin (Ω) | $2.71E-11 \mu\text{m}^3$ |
| Initial vacancy concentration (C_{v0}) | $1.11E6 \mu\text{m}^{-3}$ (Balzer and Sigvaldason, 1979) |
| Boltzmann constant | $8.62 \times 10^{-5} \text{ eV/atom K} = 1.38 \times 10^{-23} \text{ J/K}$ |
| Universal gas constant | 8.31 J/mol K |

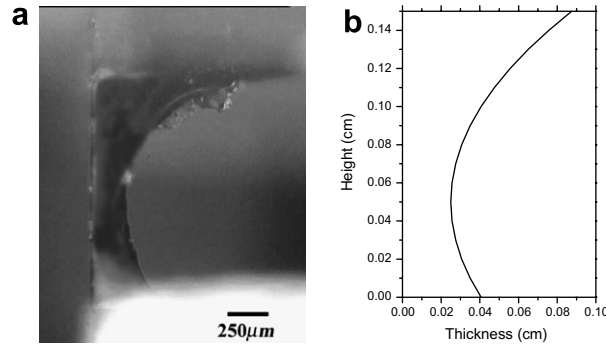


Fig. 4. (a) Optical microscopic image of the solder joint. (b) Thickness variation along the height of the solder joint used in the simulation.

$$W_{\text{thickness}} = 0.025 \times \left[1 + 2.5 \times \left(\frac{y - 0.05}{0.1} \right)^2 \right], \quad (16)$$

where y is the distance from the bottom of the solder joint. The current density variation along the height of the solder joint can be given by the following polynomial

$$j = 1.12 \times 10^4 / \left[1 + 2.5 \times \left(\frac{y - 0.05}{0.1} \right)^2 \right] \text{ (A/cm}^2\text{)}. \quad (17)$$

In order to prove the accuracy of current distribution function given in Eq. (17), a 3D electromagnetic analysis is performed using ABAQUS. The steady state result of electrical potential is shown in Fig. 5. The FE analysis verified that the current density formulation above is close to real distribution.

High sensitivity moiré interferometry technique is used for measuring displacement field during loading. The measured displacement fields in the solder joint is represented by the fringe fields, shown in Figs. 6a and b. Figs. 6d and e show deformation field results for numerical simulation after 600 h of current testing. In Fig. 6, displacement contours have the unit of micron. The displacement field predicted by numerical analysis and test data are close to each other. From the deformation mode of the solder joint shown in Fig. 6f, it is obvious that, the upper part of solder joint is in expansion and lower part of solder is in contraction. This can be explained by looking at the current density distribution which correspondence to the solder joint thickness distribution shown in Fig. 4b. In Fig. 4, current density reach a maximum value around $y = 0.5$ mm. According to Eq. (3), vacancy flux is proportional to current density, The vacancy flux increases and reaches maximum value around $y = 0.5$ mm. At the upper part of solder joint, the vacancy flux is smaller than vacancy flux at the lower part. The vacancy flow is in the same direction as current direction (from top to bottom), this means more vacancy is leaving out upper part than coming in, and as a result there exists a positive vacancy flux divergence at the upper part. The mass accumulation at the upper part of the solder joint results in expansion. The opposite happens in the lower part of the solder joint. In this simulation, since the vacancy flux

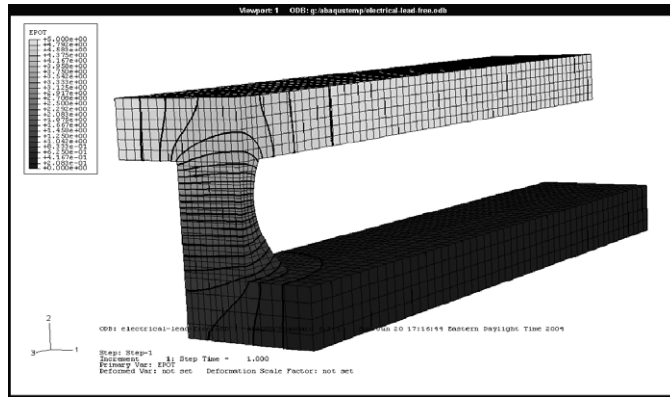


Fig. 5. Steady state electrical potential distribution for solder joint.

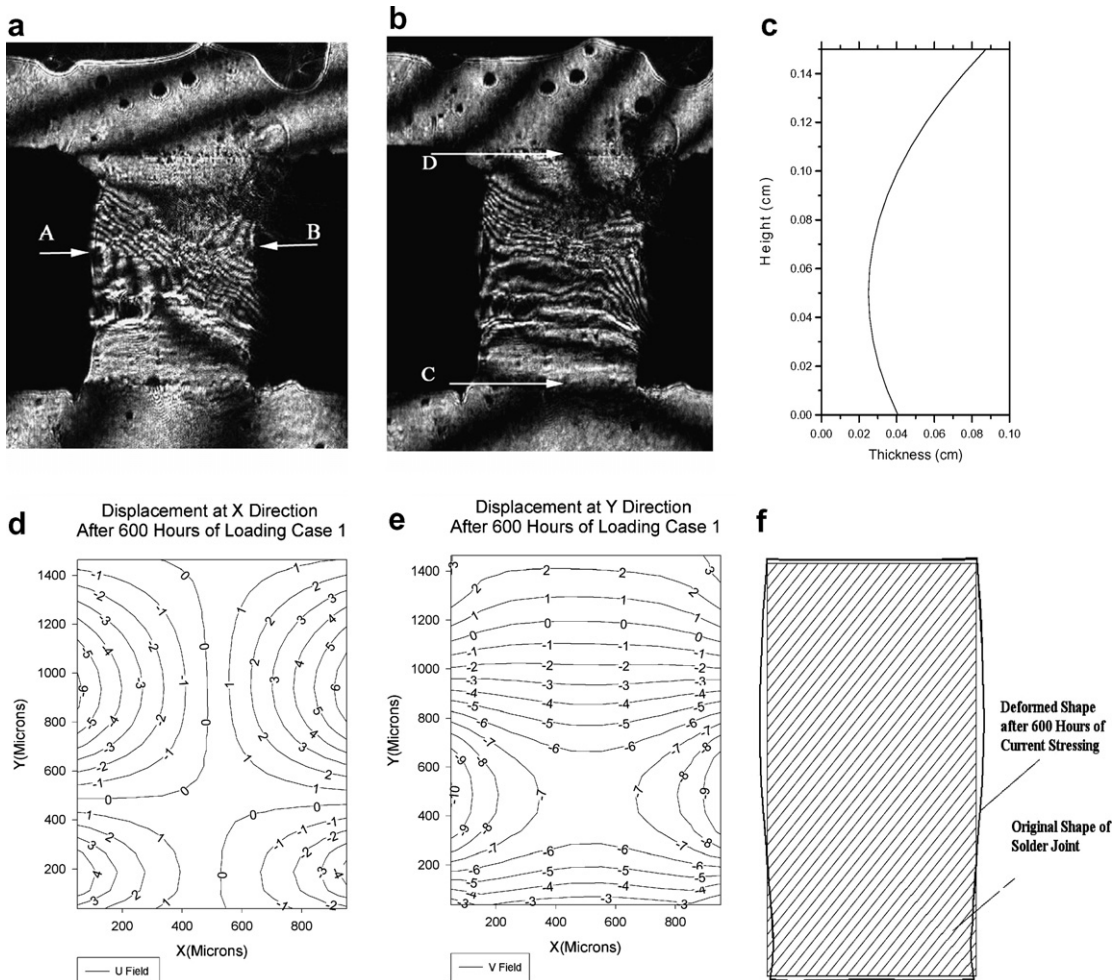


Fig. 6. (a) U-field test result. (b) V-field test result after 600 h. (c) Thickness profile of the solder joint. (d) U field (horizontal relative displacement) simulation results. (e) V field (vertical relative displacement) simulation result. (f) Deformation of simulation result. (Displacement unit for contours given in (d) and (e) is micron.) In moiré interferometry u and v fields refer to horizontal and vertical relative displacement fields, respectively.

boundary conditions of solder joint and copper plates are set up to allow for vacancy inter diffusion, the main deformation is not determined by the blocking boundary conditions, instead it is determined by current density gradient or so-called current crowding effect (Tu, 2003, 2004).

Relative displacements along vertical 2 (y) direction (V field) between Points C and D (points depicted in Fig. 6b) are shown in Figs. 7a and b. Fig. 7c shows relative horizontal deformation (U field) between points A and B. The simulation successfully predicts U and V field evolution and spatial distribution. Fig. 8 shows a comparison of FE simulation and moiré measurements for vertical (axis 2 in Fig. 3) strain distribution along the height of the solder joint.

Blech and Herring (1976) was first to prove the existence of counter vacancy flow by spherical stress gradient and vacancy gradient during electromigration. Fig. 9 indicates that the forces generated by vacancy gradient and spherical stress gradient are in the opposite direction of electrical current driving force. In order to estimate the magnitude of the forces generated by those three factors, a simple calculation is performed. The gradients are calculated based on the data provided by Fig. 9 as follows:

$$\text{Vacancy concentration gradient force; } \nabla c = \frac{1.03 - 0.90}{-1500} = -8.67 \times 10^{-5} (1/\mu\text{m}),$$

$$\text{Stress gradient force } \frac{cf\Omega}{kT} \nabla \sigma_{\text{spherical}} = \frac{1.0 \cdot 0.6 \cdot 2.71 \times 10^{-11}}{1.38 \times 10^{-11} \cdot 300} \frac{1 - (-12)}{-1500 \mu\text{m}} = -3.405 \times 10^{-5} (1/\mu\text{m}),$$

$$\text{Electrical current field force } \frac{Z^*e}{kT} (-\rho\mathbf{j})c = \frac{10 \cdot 1.602 \times 10^{-19}}{1.38 \times 10^{-11} \cdot 300} \cdot 1.15 \times 10^{11} \cdot 1.12 \times 10^{-4} \cdot 1.0 = 4.984 \times 10^{-3} (1/\mu\text{m}).$$

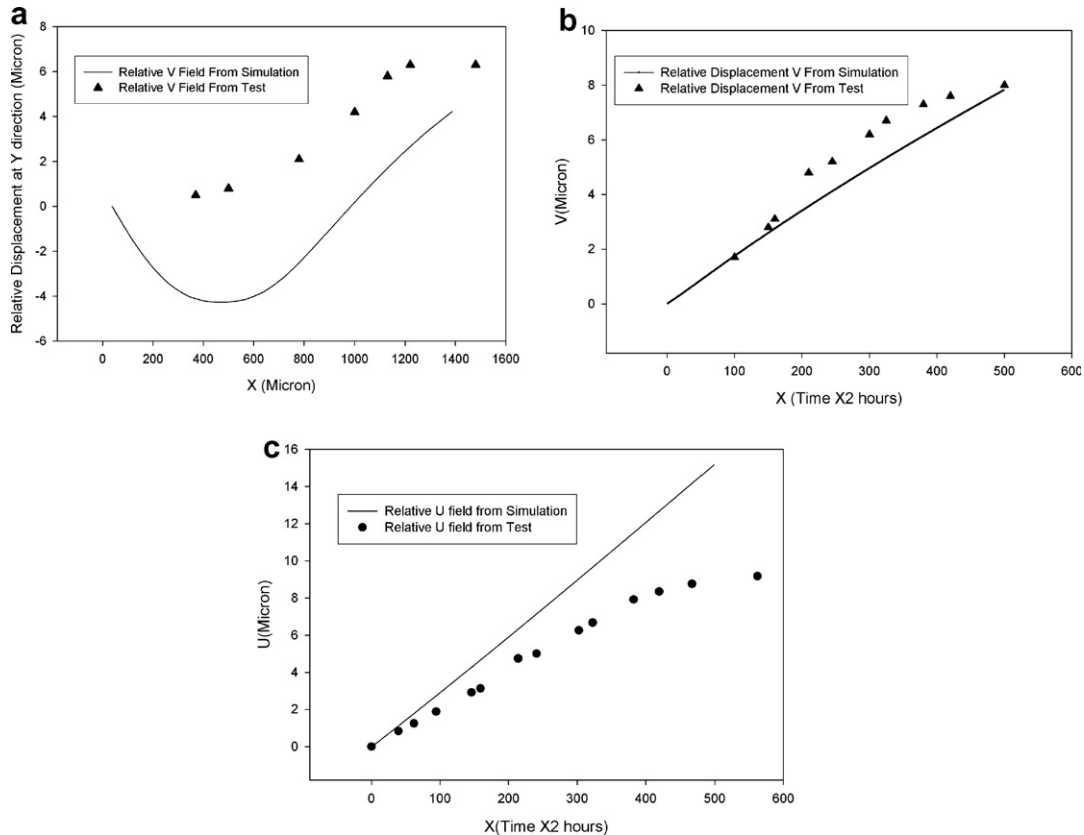


Fig. 7. (a) Relative V field distribution along Y axis between Points D and C after 600 h. (b) Relative V field displacement evolution between Points D and C. (c) Relative U field displacement evolution between Points A and B.

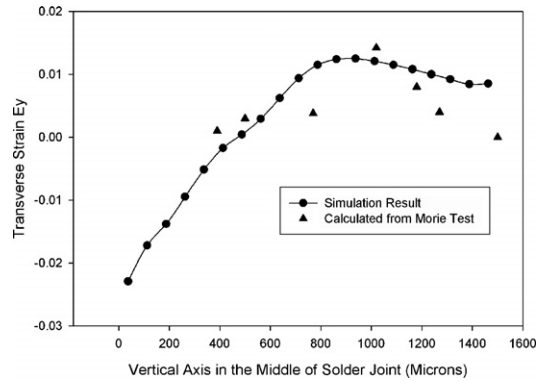


Fig. 8. Strain_Y distribution along line CD after 600 h.

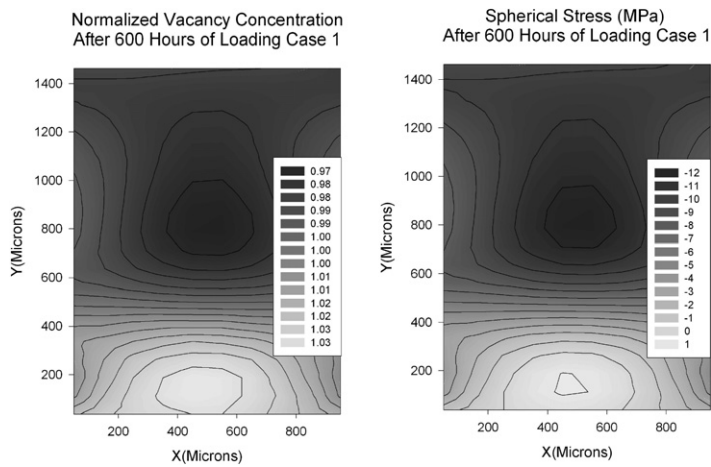


Fig. 9. Normalized vacancy concentration and spherical stress simulation results after 600 h.

The counter flow due to concentration gradient and spherical stress gradient are only 2.4% of electrical current field forces, according to above calculations. This is because of the dimension of the solder joint is large compared to 100 microns diameter found in flip chip solder joints. Diffusion in the bigger solder joints takes much longer time and also the gradient depends on dimension of the solder joint. Moreover the non blocking boundary conditions contribute to this small gradient of force and vacancy concentration. So the critical stress points (where stress driven migration stops electromigration) as stated in Blech’s paper [Blech, 1998](#) cannot be reached in this system. But this does not mean that steady state cannot be reached, the solder joints will reach a steady state once all the diffusion caused deformations cease to grow inside the solder. At the steady state although vacancy flux still exists, the vacancy flux divergence is zero everywhere.

Fig. 10 shows the total strain field distributions in horizontal 1 (X), and vertical 2 (Y) directions and shear strain. Shear strain is highly localized at the corners of solder joints and is very small at other parts of the solder joint.

In Fig. 10, the location where the strains in direction 1 (X) and direction 2 (Y) both equal to zero is a neutral axis. This corresponds to $y = 0.5$ mm where current density gradient is zero. This again proves that the deformation is primarily due to current crowding effect.

The biggest advantage of the proposed model is taking into accounts plastic deformation. Fig. 11 shows the plastic strain in X , Y directions and plastic shear strain. The major plastic strain direction is on Y direction which corresponds to major loading direction. The maximum plastic strain of Y is on the order of 3.3%. Plastic shear strain appears the same highly localized behavior as total shear strain.

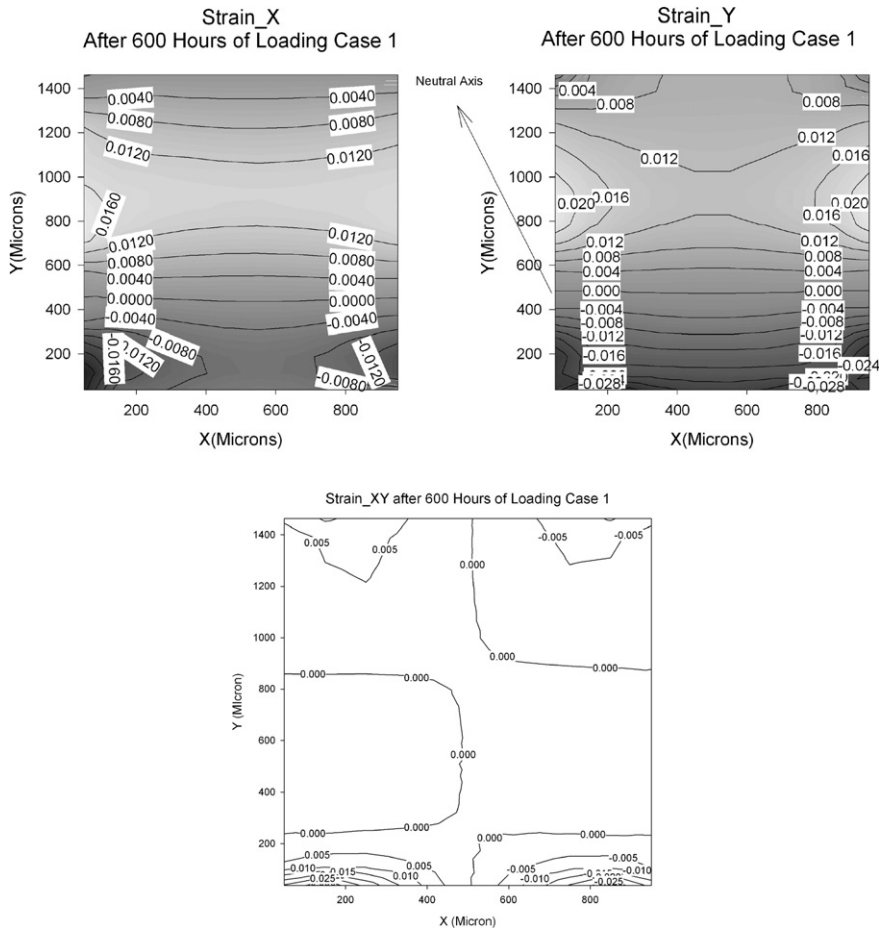


Fig. 10. Total strain field distributions after 600 h of current stressing.

In order to verify the nonlinear behavior of solder alloy under high current density, stress and total strain curves for 1000 h of simulation are shown in Fig. 12. The stress and strain data shown in Fig. 12 is for point C (defined in Fig. 6b). Here tension stress is positive and compression is negative. We can clearly see the nonlinear behavior in Fig. 12. Mass depletion happens at point C due to current direction and current crowding. Since the confinement of copper plate in direction 1 (X) is very strong, the stress in X direction is major force here and it resists the contraction of solder and solder joint appears to be as in tension. Stress in Y direction appears tension first due to the confinement in Y direction then it turns into compression. This can be explained as follows. Two copper plates can be viewed as two cantilever beams, in Y direction, it allows the solder joint to deform vertically but horizontal they provide much stronger confinement. As time evolves, eventually stress in Y direction is dominated by the stress in X direction due to Poisson’s effect and becomes compression. The stress at X direction is one order of magnitude larger than stress at Y direction from Fig. 12. Shear stress strain curve appears softening due the viscoplastic nature of stress relaxation.

4.2. Numerical simulation case 2

The current loading profile for case 2 is as follows:
 The thickness distribution along the vertical Y axis is

$$W_{\text{thickness}} = 0.025 \times \left(1 + 0.5 \times \left(\frac{y - 0.1}{0.1} \right)^2 \right) \text{ (A/cm}^2\text{)} \quad (18)$$

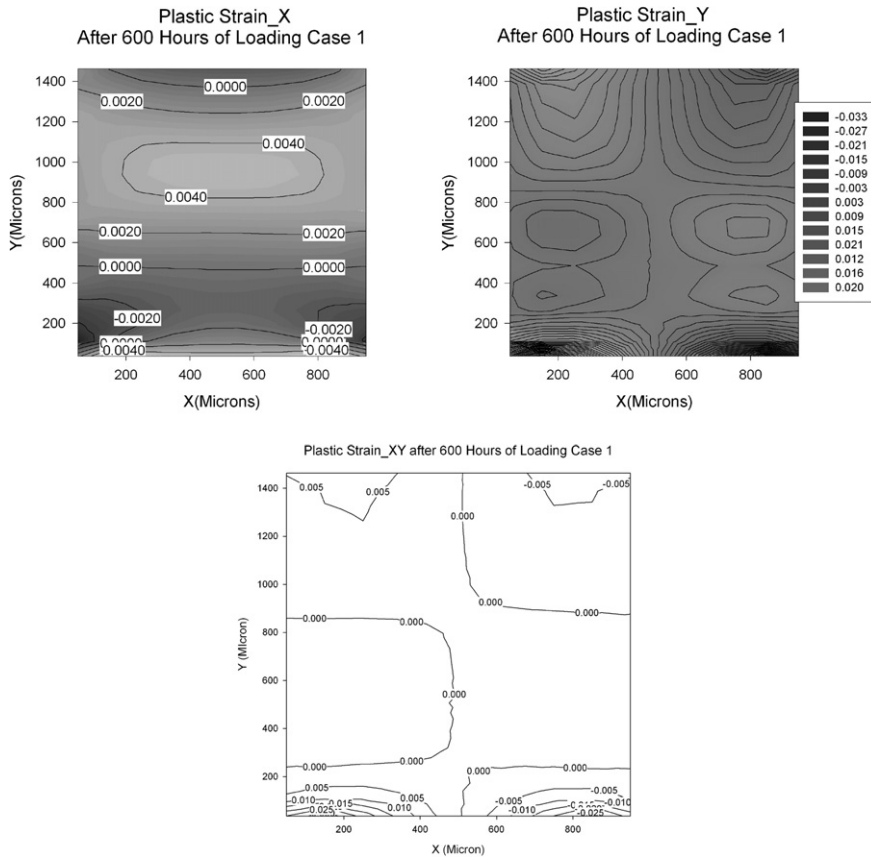


Fig. 11. Plastic strain deformation fields after 600 h.

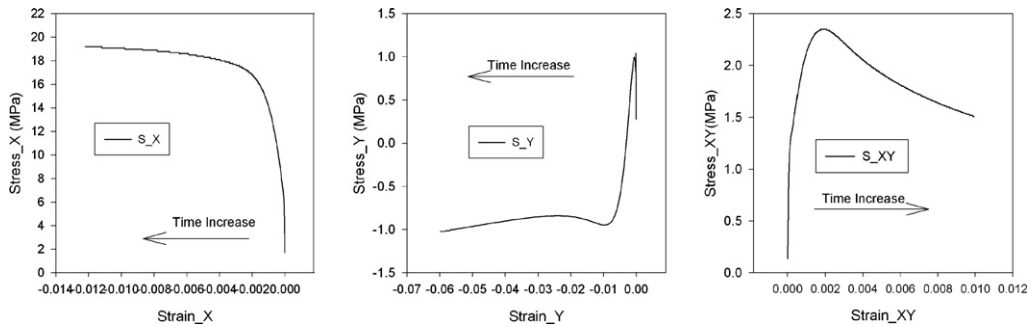


Fig. 12. Strain–stress evolutions for 1000 h simulation.

average current density is 6000 A/cm². The current density distribution is

$$j = 0.6 \times 10^4 / \left(1 + 0.5 \times \left(\frac{y - 0.1}{0.1} \right)^2 \right) \text{ (A/cm}^2\text{)}. \tag{19}$$

The neutral axis is around $y = 1$ mm for the current density distribution shown above. The current density in case 2 is smaller than the case 1 and the current crowding effect is weaker than case 1.

The displacement fields shown in Fig. 13 is similar to case 1 where as in solder joint 1, the upper part of solder joint (anode) is in expansion and lower part of solder joint is in contraction in X direction. The relative

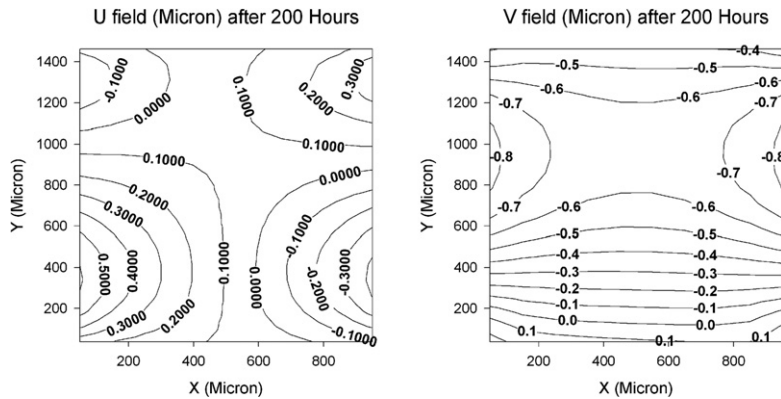


Fig. 13. Displacement fields distribution for solder joint 2 after 200 h.

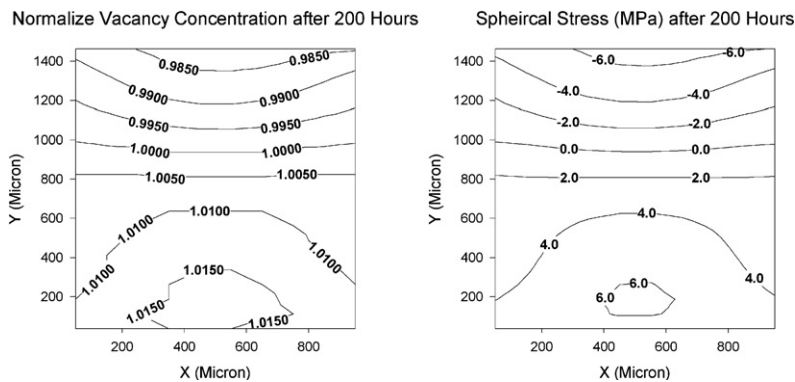


Fig. 14. Normalize vacancy concentration and spherical stress for solder 2 after 200 h.

displacement between points C and D (points are shown in Fig. 6) is $0.5360 \mu\text{m}$ from simulation results and moiré interferometry measured value is $0.834 \mu\text{m}$. Relative displacement between points A and B is $0.5233 \mu\text{m}$ and moiré measured value is $0.834 \mu\text{m}$. Since precision of Moiré interferometry limited by the frequency of the diffraction grating (1200 lines/mm) which is $0.417 \mu\text{m}$ per fringe order, the discrepancy between test and simulation is within the error limit of moiré interferometry technique. The displacement in case 2 is smaller than case 1 because of current density and current density gradient are both smaller than case 1.

Normalized vacancy concentration and spherical stress distributions after 200 h of current stressing for case 2 are shown in Fig. 14. The driving forces by spherical stress gradient and vacancy gradient are on the opposite direction of current driving forces as expected. Fig. 15 shows the strain fields including total strains and plastic strains for case 2 after 200 h. Around $y = 1 \text{ mm}$ horizontal line, strains are zero as expected since at this location the gradient of current density is zero. The order of plastic strain fields and shear total strain are in the range of 1×10^{-4} . The total strain fields except shear plastic strain are on the order of 1×10^{-3} .

Fig. 16 shows the total strain and stress evolution curves for case 2 at 250 h of current loading at point C. All three components of stresses exhibit the same hardening behavior after yielding. The mechanical behaviors of lead-free solder joints are consistent by comparing stress strain curves shown in Fig. 12 with Fig. 16.

5. Conclusions

A constitutive model for electromigration induced deformation is proposed and implemented in ABAQUS. Simulations are performed for lead-free solder joints under high current density loadings. By incorporating plasticity into electromigration model, this model has the capability of simulating proper mechanical response

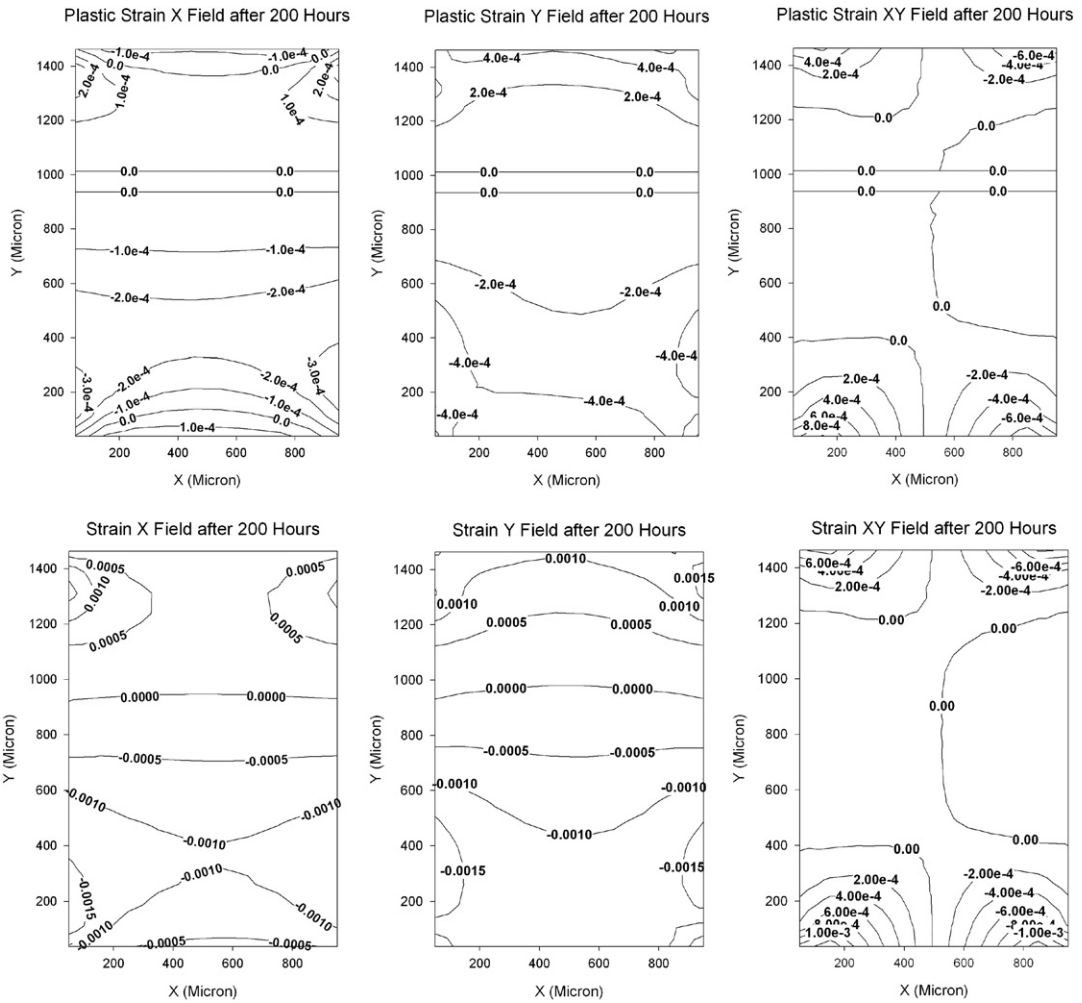


Fig. 15. Strain fields distribution after 200 h for solder 2.

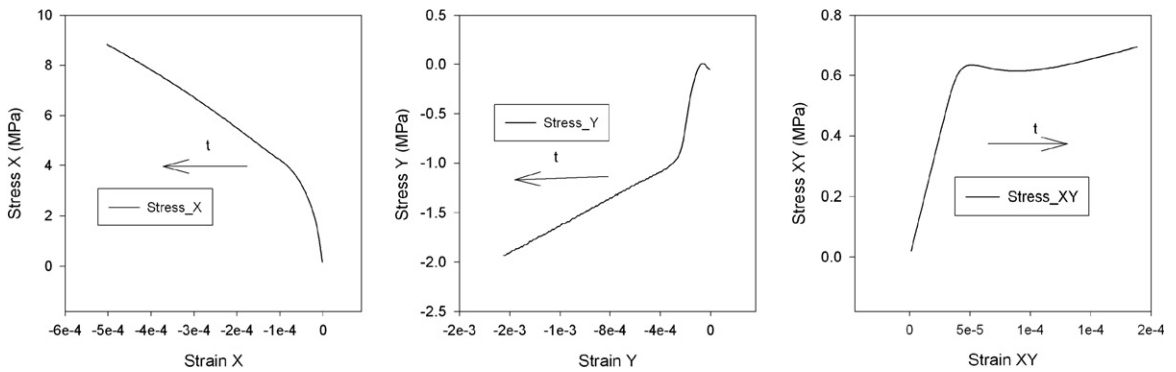


Fig. 16. Stress–strain evolution of solder 2 for 250 h current loading.

under electromigration since the assumption of elasticity can not hold for most of the cases under electromigration. Most importantly this study shows that contrary to popular belief, there is significant plasticity due to electromigration.

Two cases of lead-free joints under different current density profiles are simulated and results are compared with experimental moiré interferometry measurements. The comparisons indicate that there is a very good match between simulation and test results. The simulation confirmed that current density gradient (current crowding) is the major source of flux divergence under non blocking boundary conditions. A 3D electromagnetic steady state analysis is performed to verify the current density profile. The non-blocking boundary condition is due to the fact that copper inter diffuses with tin to form intermetallic compounds (Choi et al., 2002).

With the proper consideration for material mechanical behavior, the stress and vacancy distribution can be simulated with a high degree of confidence. This will improve the electromigration simulation accuracy and gives us a tool for prediction and verification of certain material properties related to electromigration, for example, the determination of effective charge number. Parametric study can be utilized to obtain value of effective charge number to match up with experimental observation.

The simulation of plastic strain and stress behavior also reveals material damage evolution process. Both stress and plastic strain are related to damage of material. The simulation thus can be utilized to simulate material degradation process with certain damage criteria (Basaran et al., 2003). Numerical analysis error in this analysis may come from several aspects

(1) Material parameters, like diffusivity and effective charge number values scatter a lot in the literature. This can be improved by comparing more test and simulation cases to reach certain confidence in material parameters. Unfortunately there is very little data, if any, on electromigration of lead-free solder alloys.

(2) Structure modeling, using plain strain with thickness brings some degree of error. A 3D analysis would improve the result it but is much more time consuming.

(3) Numerical error inherited in finite element simulation, which can be improved with finer mesh but also requires more computational time. This is verified by mesh sensitivity analysis conducted for aluminum electromigration cases (Lin and Basaran, 2005).

(4) Microstructural evolution and its influence are not taken into account in the current model and future development on this aspect is under way.

Acknowledgement

This research project has been sponsored by US Navy Office of Naval Research Advanced Electrical Power Systems program under the direction of Terry Ericson.

References

- Goods, S.H., Brown, L.M., 1978. The nucleation of cavities by plastic deformation. *Acta Materialia* 27, 1–15.
- Gleixner, R.J., Nix, W.D., An analysis of void nucleation in passivated interconnect lines due to vacancy condensation and interface contamination, *Materials Reliability in Microelectronics VI*, San Francisco, CA, April 8–12 1996, pp. 475–480.
- Blech, I.A., 1998. Diffusional back flows during electromigration. *Acta Materialia* 46 (11), 3717–3723.
- Park, Y.J., Andleigh, V.K., Thompson, C.V., 1999. Simulations of stress evolution and the current density scaling of electromigration-induced failure times in pure and alloyed interconnects. *Journal of Applied Physics* 85 (7), 3546–3555.
- Ye, H., Basaran, C., Hopkins, D., 2003. Numerical simulation of stress evolution during electromigration in IC interconnect lines. *IEEE Transactions on Components and Packaging Technologies* 26 (3), 673–681.
- Korhonen, M.A., Børgesen, P., Tu, K.N., Li, C.-Y., 1993. Stress evolution due to electromigration in confined metal lines. *Journal of Applied Physics* 73 (8), 3790–3799.
- Sarychev, M.E., Zhinikov, V. Yu, 1999. General model for mechanical stress evolution during electromigration. *Journal of Applied Physics* 86 (6), 3068–3075.
- Lin, M., Basaran, C., 2005. Electromigration induced stress analysis using fully coupled mechanical and diffusion finite element analysis with non linear material properties. *Computational Material Science* (34/1), 82–98.
- Lubarda, V.A., Benson, D.J., 2002. On the numerical algorithm for isotropic-kinematic hardening with the Armstrong–Frederick evolution of the back stress. *Computer Methods in Applied Mechanics and Engineering* 191 (33), 3583–3596.
- Basaran, C., Lin, M., Ye, H., 2003. A thermodynamic model for electrical current induced damage. *International Journal of Solids and Structures* 40 (26), 7315–7327.
- Neu, R.W., Scott, D.T., Woodmansee, M.W., 2000. Measurement and modeling of back stress at intermediate to high homologous temperatures. *International Journal of Plasticity* 16 (3–4), 283–301.
- McDowell, D.L., 1992. A nonlinear kinematic hardening theory for cyclic thermoplasticity and thermoviscoplasticity. *International Journal of Plasticity* 8 (6), 695–728.

- Armstrong, P.J., Frederick, C.O., A mathematical representation of the multiaxial Bauschinger effect, G.E.G.B. Report RD/B/N731, 1966.
- Chaboche, J.L., 1989. Constitutive equations for cyclic plasticity and cyclic viscoplasticity. *International Journal of Plasticity* 5 (3), 247–302.
- Ye, H., Basaran, C., Hopkins, D.C., 2004. Deformation of solder joint under current stressing and numerical simulation – I. *International Journal of Solids and Structures* 41, 4939–4958.
- Ye, H., Basaran, C., Hopkins, D., 2003. Mechanical degradation of solder joints under current stressing. *International Journal of Solids and Structures* 40 (26), 7269–7284.
- Ye, H., Basaran, C., Hopkins, D.C., 2004. Deformation of microelectronic solder joints under current stressing and numerical simulation II. *International Journal of Solids and Structures* 41, 4959–4973.
- Balzer, R., Sigvaldason, H., 1979. Equilibrium vacancy concentration measurements on tin single crystals. *Physica Status Solidi B: Basic Research* 92 (1), 143–147.
- Prabjit, S., Milton, O., 1984. Tracer study of diffusion and electromigration in thin tin films. *Journal of Applied Physics* 56 (4), 899–907.
- Clement, J.J., Thompson, C.V., 1995. Modeling electromigration-induced stress evolution in confined metal lines. *Journal of Applied Physics* 78 (2), 900–904.
- Tu, K.N., 2003. Recent advances on electromigration in very-large-scale-integration of interconnects. *Journal of Applied Physics* 94 (9), 5451–5473.
- Blech, I.A., Herring, C., 1976. Stress Generation by electromigration. *Applied Physics Letters* 29 (3), 131–133.
- Choi, W.J., Yeh, E.C.C., Tu, K.N., Elenius, P., Balkan, H., Electromigration of flip chip solder bump on Cu/Ni(V)/Al thin film under bump metallization. In: 52nd Electronic Components and Technology Conference 2002 (Cat. No. 02CH37345). IEEE 2002, Piscataway, NJ, USA, 2002, pp. 1201–1205.
- Ye, H. Mechanical Behavior of Microelectronics and Power Electronics Solder Joints Under High Current Density: Analytical modeling and Experimental Investigation,” PhD Dissertation submitted to State University of New York at Buffalo, 2004.